

Fitting all parameters of the Quermass model by the Takacs-Fiksel method

David DEREUDRE

LAMAV, Université de Valenciennes et du Hainaut-Cambrésis
Le Mont Houy
59313 Valenciennes Cedex 09, France
e-mail : david.dereudre@univ-valenciennes.fr

Frédéric LAVANCIER

Université de Nantes,
Laboratoire de Mathématiques Jean Leray,
2 rue de la Houssinière
44322 Nantes Cedex 3, France.
e-mail : frederic.lavancier@univ-nantes.fr

Kateřina STAŇKOVÁ HELISOVÁ

Czech Technical University in Prague, Faculty of Electrical Engineering,
Department of Mathematics, Technická 2,
16627 Prague 6 - Dejvice, Czech Republic.
e-mail : helisova@math.feld.cvut.cz

July 26, 2012

Abstract

The Quermass model is a generalization of the classical germ-grain Boolean model for which a morphological interaction is added. It allows to model random structures with specific morphologies which are unlikely to come from a Boolean model. The Quermass model depends on three interacting parameters and on an intensity parameter. Since the number of points is not observable from a germ-grain set, the estimation of all parameters is not possible from classical likelihood or pseudo-likelihood approaches. In this paper, we present a procedure based on the Takacs-Fiksel method which is able to fit all parameters of the Quermass model, included the intensity. An intensive simulation study is conducted to assess the efficiency of the procedure and to provide practical recommendations. An application to heather data, initially studied by P. Diggle, is finally proposed.

KEY-WORDS: Gibbs Point Process, germ-grain model, Quermass-Interaction Process, Area-Process, Perimeter-Process, Takacs-Fiksel estimator.

1 Introduction

Physics, biology or agronomy are often confronted with problems involving complex random sets like liquid-vapor interface structures, micro-emulsions, porous media or propagation domains of plants. Admissible models for these random structures are the germ-grain models, which consist in the union of locally finite random sets called grains. The most popular germ-grain model is certainly the Poisson Boolean model of balls. In this model, the grains correspond to balls, whose centers are distributed as a Poisson point process and the radii are independently and identically distributed. The probabilistic and statistical properties of the Boolean model have been widely studied (see for example [16], [27]). However, the variety of morphological structures induced by the Boolean model is limited. To reach more realistic morphologies, some Gibbs modifications of the Boolean model have been developed. The rough idea is to introduce an interaction (or Hamiltonian) acting on the morphology of the random set. This leads to a new random structure which tends to minimize this Hamiltonian. In this way, some morphological features are more likely to occur than for Boolean sets.

A first morphological interaction based on the area of the germ-grain structure has been introduced in [30] to model phase transition phenomena in statistical mechanics. More complex interactions appeared later in the nineties [1, 13, 14, 15]. Hadwiger's theorem [10] ensures, under mild conditions, that any function acting on an union of compact convex sets can be decomposed into a linear combination of the Minkowski (or Quermass) functionals. These functionals correspond in \mathbb{R}^2 to the area, the perimeter and the Euler-Poincaré characteristic (number of connected components minus number of holes). Accordingly, any morphological interaction in \mathbb{R}^2 can be written as a linear combination of these three functionals. The Quermass model corresponds to the Gibbs modification of the Boolean model based on such linear interactions. From Hadwiger's theorem, it appears as a very rich model to represent random structures.

The Quermass model in \mathbb{R}^2 depends on the law of the radii and on four parameters: the three coefficients in the linear combination defining the Hamiltonian, and the intensity parameter of the underlying Boolean model. The present paper deals with the estimation of these four parameters.

The main difficulty comes from the nature of the observable data, which are the germ-grain set. In particular the positions and the number of balls are not observed and can not be used in the statistical procedure, which is untypical in estimation problems for Gibbs point processes. Note that this specific issue already occurs for the estimation of the intensity parameter of the classical Boolean model. In this case, some explicit estimating equations have been found, that express the intensity parameter in terms of the specific volume of the set, see [16]. In presence of Gibbs interactions as for the Quermass model, it is well-known that the computation of macroscopic quantities is intractable, so a similar explicit estimation procedure is not possible.

Assuming the intensity parameter of the underlying Boolean model is known, a maximum likelihood approach is investigated in [18] for the estimation of the three parameters of the Quermass interaction. Unfortunately the intensity parameter can not be fitted by this method due to the unobservability of the number of points. Section 3.1 gives more details about this procedure and explain the serious consequences of a misspecification of the intensity parameter in practice. In this paper, we fit all parameters of the Quermass process, including the intensity, via a Takacs-Fiksel procedure ([28], [7], [3]). The Takacs-

Fiksel contrast function is based on an empirical counterpart of the Georgii-Nguyen-Zessin equilibrium equation (2.3), and depends on the choice of some test functions. Due to the unobservability of points, the contrast function is not computable in general, but some specific choices of test functions overcome this issue (see Section 3.2.2). This is the key ingredient for the estimation of the Quermass model by the Takacs-Fiksel procedure. The purpose of the present paper is to develop in details this method, to provide a simulation study and to deduce some practical recommendations.

As an application, we finally fit a Quermass model to heather data. Heather dataset has been initially studied by P. Diggle in [6], followed by many studies ([11], [12], [4], [19], [18]). We show that our fitted model seems a better approximation of heather dataset, both from a visual impression and from a stastical diagnostic inspection.

In Section 2, we introduce the Quermass model and we recall the fundamental Georgii-Nguyen-Zessin equation. Section 3 presents the estimation procedures. The limitation in using the maximum likelihood approach is explained in Section 3.1. Then in Section 3.2 we present the general Takacs Fiksel procedure and its application to the Quermass model. Practical aspects for the implementation of the procedure are given in Section 4. A simulation study assessing the efficiency of the procedure is presented in Section 5. An application to heather dataset is conducted in Section 6. Note finally that an appealing alternative estimation procedure would consist in combining the likelihood and the Takacs-Fiksel approaches, to take advantages of both methods. Following this idea, we have developed a mixed procedure. But it turns out to be very time consuming without being more efficient. Its presentation is postponed to an appendix.

2 Quermass Model

2.1 Notations

We denote by \mathcal{E} the space $\mathbb{R}^2 \times [0, R_0]$ (where $R_0 > 0$ is a fixed positive real number) endowed with its natural Euclidean Borel σ -algebra. It is the space of marked points (x, R) where $x \in \mathbb{R}^2$ is the centre of a ball and R its radius. We assume for simplicity that the radii are uniformly bounded by R_0 . This assumption allows to define easily the Quermass model on the full plane \mathbb{R}^2 , see section 2.3, though this restriction is not mandatory (see [5]). For any bounded set Λ in \mathbb{R}^2 , we denote by $\mathcal{E}_\Lambda := \Lambda \times [0, R_0]$ the restriction of \mathcal{E} to Λ .

By definition, a *configuration* of points ω is a locally finite subset of \mathcal{E} , which means that the set $\omega_\Lambda := \omega \cap \mathcal{E}_\Lambda$ is finite for any bounded set Λ in \mathbb{R}^2 . The space of all configurations of points in \mathcal{E} is denoted by Ω , while for any bounded set Λ in \mathbb{R}^2 , Ω_Λ denotes the subspace of configurations included in \mathcal{E}_Λ .

For $x \in \mathbb{R}^2$, we write for short $x \in \omega$ if there exists $R \in [0, R_0]$ such that $(x, R) \in \omega$. For $(x, R) \in \mathcal{E}$ we write $\omega \cup (x, R)$ in place of $\omega \cup \{(x, R)\}$ and $\omega \setminus (x, R)$ in place of $\omega \setminus \{(x, R)\}$.

For any configuration ω we denote by \mathcal{U}_ω its germ-grain representation defined by the following set

$$\mathcal{U}_\omega := \bigcup_{(x, R) \in \omega} B(x, R),$$

where $B(x, R)$ is the closed ball centered at x with radius R .

Let μ be a reference probability measure on $[0, R_0]$. We denote by λ the Lebesgue measure on \mathbb{R}^2 and by π^μ the marked Poisson process on \mathcal{E} with intensity measure $\lambda \otimes \mu$. For every bounded set Λ , the probability measure π_Λ^μ denotes the marked Poisson process on \mathcal{E}_Λ with intensity measure $\lambda_\Lambda \otimes \mu$. Recall that the law of the random set \mathcal{U}_ω under the probability measure π^μ is nothing else than the standard homogeneous Boolean model with intensity one and distribution of radii μ .

2.2 Quermass model on a bounded window Λ

Following Kendall et al. [13], for any configuration ω_Λ in a bounded window Λ in \mathbb{R}^2 , the Quermass-interaction (or Quermass Hamiltonian) is defined by

$$H^\theta(\omega_\Lambda) = \theta_1 \mathcal{A}(\mathcal{U}_{\omega_\Lambda}) + \theta_2 \mathcal{L}(\mathcal{U}_{\omega_\Lambda}) + \theta_3 \chi(\mathcal{U}_{\omega_\Lambda}), \quad (2.1)$$

where $\theta := (\theta_1, \theta_2, \theta_3)$ is a vector of real parameters. The functionals \mathcal{A} , \mathcal{L} and χ are the three fundamental Minkowski (or Quermass) functionals: area, perimeter and Euler-Poincaré characteristic (number of connected components minus the number of holes).

From Hadwiger's Theorem [10], any additive functional F defined on the space of finite unions of convex compact sets (i.e. $F(A \cup B) = F(A) + F(B) - F(A \cap B)$) and satisfying some continuity assumption (see [10]) can be decomposed as in (2.1). This universal representation explains the interest of the Quermass interaction for morphological model at mesoscopic scale [14, 15].

Definition 2.1. *The Quermass point process on a bounded set Λ in \mathbb{R}^2 for the parameter θ , the intensity $z > 0$ and the distribution of radius μ is the probability measure $P_\Lambda^{z, \theta}$ on Ω_Λ which is absolutely continuous with respect to the marked Poisson Process π_Λ^μ with density*

$$g_\Lambda(\omega_\Lambda; z, \theta) = \frac{1}{Z_\Lambda(z, \theta)} z^{n(\omega_\Lambda)} e^{-H^\theta(\omega_\Lambda)},$$

where $Z_\Lambda(z, \theta) := \int z^{n(\omega_\Lambda)} e^{-H^\theta(\omega_\Lambda)} \pi_\Lambda^\mu(d\omega_\Lambda)$ is a normalizing constant called the partition function.

Some simulations are displayed in Figure 1. They correspond to Quermass models involving only one non-null interacting parameter: the Area process ($\theta_2 = \theta_3 = 0$), the Perimeter process ($\theta_1 = \theta_3 = 0$), and the Euler-Poincaré process ($\theta_1 = \theta_2 = 0$). These extreme situations show the rich variety of random sets that Quermass processes can provide. Note that in the three situations displayed in Figure 1, the interacting parameter is positive, so that the resulting random set is more likely to induce a lower Minkowski functional (resp. \mathcal{A} , \mathcal{L} or χ) than in the Boolean case. These simulations have been done by a birth-death Metropolis-Hasting algorithm as presented in [17].

2.3 The Gibbs property: Quermass model on the full plane

In this section the Gibbs (or Markov) property of the Quermass model is displayed via the Georgii-Nguyen-Zessin (GNZ) equation. Another equivalent and certainly more natural presentation could have been considered via the DLR equations. But the latter point view requires to introduce more technical materials, that we do not use in this work, so we decided to focus on the GNZ perspective. We refer to [8, 23, 25] for details about the

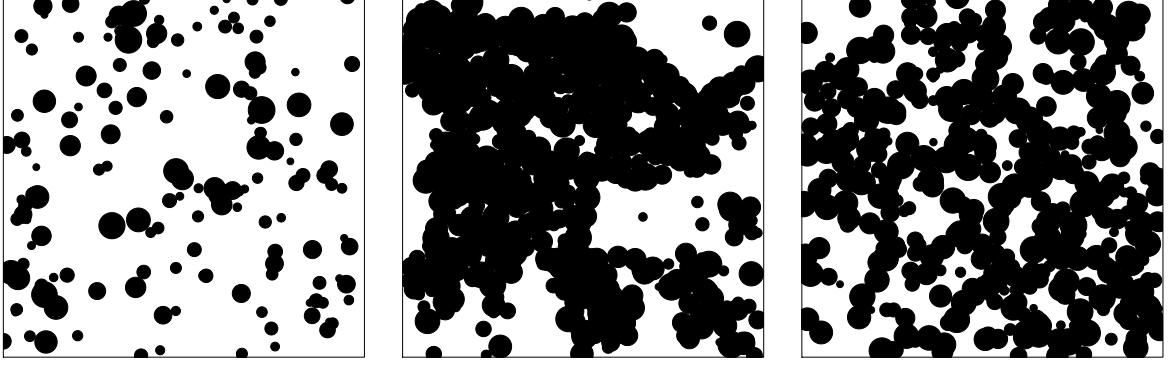


Figure 1: Samples of: the Area process with $z = 0.1$, $\theta_1 = 0.2$ (left); the Perimeter process with $z = 0.2$, $\theta_2 = 0.4$ (middle); the Euler-Poincaré process with $z = 0.1$, $\theta_3 = 1$ (right). The window is $[0, 50]^2$ and the radii are uniformly distributed on $[.5, 2]^2$.

general theory of Gibbs point processes with, in particular, a presentation via the DLR equations.

First, let us define the local energy of a marked point (x, R) with respect to a configuration ω by the following expression

$$h^\theta((x, R), \omega) := H^\theta(\omega_\Delta \cup (x, R)) - H^\theta(\omega_\Delta), \quad (2.2)$$

where Δ is any bounded set containing the ball $B(x, 2R_0)$. Thanks to the additivity of the functionals \mathcal{A} , \mathcal{L} and χ , this local energy does not depend on the choice of such Δ , so we can simply choose $\Delta = B(x, 2R_0)$. Note that the local energy is related to the Papangelou intensity

$$\lambda^*((x, R), \omega) := \frac{g_\Delta(\omega_\Delta \cup (x, R); z, \theta)}{g_\Delta(\omega_\Delta; z, \theta)},$$

where Δ satisfies the same condition as above, by $\lambda^*((x, R), \omega) = \exp(-h^\theta((x, R), \omega))$.

We have the following characterisation of the Quermass process via the Georgii-Nguyen-Zessin equation (GNZ equation).

Proposition 2.2 (Georgii [8], Nguyen-Zessin [21]). *For any bounded set Λ , a probability measure P on Ω_Λ is the Quermass point process on Λ for the parameter θ , the intensity $z > 0$ and the distribution of radius μ (i.e. $P = P_\Lambda^{z, \theta}$) if and only if for any non-negative function f from $\Omega_\Lambda \times \mathcal{E}$ to \mathbb{R}*

$$\mathbb{E} \left(\sum_{x \in \omega_\Lambda} f((x, R), \omega_\Lambda \setminus (x, R)) \right) = \mathbb{E} \left(\int_0^{R_0} \int_\Lambda z e^{-h^\theta((x, R), \omega_\Lambda)} f((x, R), \omega_\Lambda) dx \mu(dR) \right), \quad (2.3)$$

where \mathbb{E} denotes the expectation with respect to P .

The GNZ-equation involves the expectation under the Quermass process of two completely different expressions. This equilibrium equation is the starting point of the Takacs-Fiksel estimation procedure presented in Section 3.2.

In the present paper, we mainly consider Quermass processes on bounded windows as presented in definition 2.1. However, it is necessary to consider Quermass processes on the full plane \mathbb{R}^2 for questions involving asymptotic properties of estimators (as consistency or asymptotic normality). This extension is not trivial since the energy $H^\theta(\omega)$ in (2.1) of an infinite configuration ω in \mathbb{R}^2 does not exist in general and so the definition 2.1 makes no sense in this case. A definition of the Quermass process on \mathbb{R}^2 is possible thanks to the GNZ-equation (2.3).

Definition 2.3. *A probability measure $P^{z,\theta}$ on Ω is a Quermass point process on \mathbb{R}^2 for the parameter θ , the intensity $z > 0$ and the distribution of radius μ if for any non-negative function f from $\Omega \times \mathcal{E}$ to \mathbb{R} , for any bounded set Λ in \mathbb{R}^2 ,*

$$\mathbb{E} \left(\sum_{x \in \omega_\Lambda} f((x, R), \omega \setminus (x, R)) \right) = \mathbb{E} \left(\int_0^{R_0} \int_\Lambda z e^{-h^\theta((x, R), \omega)} f((x, R), \omega) dx \mu(dR) \right),$$

where \mathbb{E} denotes the expectation with respect to $P^{z,\theta}$.

The existence of a measure $P^{z,\theta}$ satisfying definition 2.3, its uniqueness or non-uniqueness (i.e. the occurrence of phase transition) are difficult problems of statistical physics. The existence has been proved recently for any $z > 0$ and any $\theta \in \mathbb{R}^3$ in [5]. The uniqueness of $P^{z,\theta}$ depends on the values of the parameters and very few is known about this issue. For the area process (i.e. $\theta_2 = \theta_3 = 0$) and when the radii are not random (i.e. $\mu(\{R_0\}) = 1$), a phase transition has been proved to occur in the very particular case where $\theta_1 = z$ and z is large enough ([2, 30]).

3 The estimation procedures

Let us consider a realisation ω of a Quermass point process P^{z^*,θ^*} defined on Λ' , where $\Lambda' \subseteq \mathbb{R}^2$, and where z^* and θ^* are unknown. In practice, one only observes the random set $\mathcal{U}_\omega \cap \Lambda$ in a bounded window $\Lambda \subseteq \Lambda'$, and not ω_Λ . So the positions of the marked points (x, R) in ω_Λ are unknown. A challenging task is then to estimate the parameters $z^* > 0$ and $\theta^* = (\theta_1^*, \theta_2^*, \theta_3^*)$ in presence of this unobservability issue, which is an unusual problem of inference for Gibbs point processes. The first subsection explains the limitation in using the maximum likelihood procedure (MLE). The second subsection focuses on the main approach of this paper which is the Takacs-Fiksel (TF) method. An attempt to combine MLE and TF procedures is displayed in appendix. We assume all along this paper that the distribution of the radii μ is known.

3.1 The maximum likelihood approach

When z^* is known, the classical maximum likelihood approach let the estimation of the parameter θ^* possible. This has been investigated in [18], where the authors introduce an original procedure based only on the connected components that are completely included in the observation window. The boundary effects are then limited. However, the maximum likelihood procedure does not allow us to fit the intensity parameter z^* since the number of points is unobservable. If z^* is unknown, a two step procedure is proposed in [18]: first estimating z^* as if the observable data come from a Boolean model (various methods are

available in this setting), then, in a second step, applying the MLE procedure to estimate θ^* .

Unfortunately, it seems that this two step procedure induces a strong restriction on the possible values for the interacting parameter θ^* . Indeed, in the first step, the estimation \hat{z} is chosen such that the Boolean model with intensity \hat{z} has the same specific volume than the observed real data. Similarly, in the second step, the MLE estimation of θ^* ensures that the corresponding Quermass process has the same specific volume than the real data. So, this two step procedure concerns Quermass processes with intensity parameter \hat{z} , that exhibit the same specific volume as the Boolean model with intensity \hat{z} . This turns out to be a strong restriction. For example, it is well-known that the Area process (i.e. $\theta_2^* = \theta_3^* = 0$) with parameters z^* and $\theta_1^* > 0$ is strictly stochastically dominated by the Boolean model with intensity z^* [9], which implies a strict comparison of their specific volumes. For this example, the lonely possible value of θ_1^* following the previous restriction is thus $\theta_1^* = 0$.

3.2 The Takacs-Fiksel approach

The possibility to use the Takacs-Fiksel procedure for fitting all parameters of the Quermass process, including z^* , has been recently emphasized in [3]. In this section we recall the procedure, which depends on the choice of some test functions. Next we display various test functions, which allow to overcome the unobservability issue of the Quermass model.

3.2.1 The general procedure

Consider, for any non-negative function f from $\Omega \times \mathcal{E}$ to \mathbb{R} , the random variable

$$C_\Lambda^{z,\theta}(\omega; f) = \sum_{x \in \omega_\Lambda} f((x, R), \omega \setminus (x, R)) - \int_0^{R_0} \int_\Lambda z e^{-h^\theta((x, R), \omega)} f((x, R), \omega) dx \mu(dR). \quad (3.1)$$

From the ergodic theorem, if Λ is large enough, $C_\Lambda^{z,\theta}(\omega; f)/|\Lambda|$ is approximatively equal to $\mathbb{E}_{z^*, \theta^*}(C_{[0,1]^2}^{z,\theta}(\omega; f))$, where $\mathbb{E}_{z^*, \theta^*}$ is the expectation with respect to P^{z^*, θ^*} . Moreover, from the GNZ equation (2.3) it is easy to show that $\mathbb{E}_{z^*, \theta^*}(C_{[0,1]^2}^{z^*, \theta^*}(\omega; f)) = 0$. Therefore, for any function f , the random variable in (3.1) should be close to zero when $z = z^*$ and $\theta = \theta^*$. This remark is the basis of the Takacs-Fiksel approach.

Let us give K functions $(f_k)_{1 \leq k \leq K}$, the Takacs-Fiksel estimator is simply defined by

$$(\hat{z}, \hat{\theta}) := \arg \min_{z, \theta} \sum_{k=1}^K \left(C_\Lambda^{z,\theta}(\omega; f_k) \right)^2. \quad (3.2)$$

The strong consistency and asymptotic normality of $(\hat{z}, \hat{\theta})$ when the observation window Λ grows to \mathbb{R}^2 are discussed in [3]. The main ingredient for consistency is to ensure that (z^*, θ^*) is the unique solution to the optimisation problem in (3.2) when Λ is large enough. This identifiability is not easy to check. Some criteria are given in [3]. If p is the number of parameters to estimate, it turns out that choosing $K = p$ test functions may be not sufficient to guaranty identifiability. If $K > p$, then identifiability is in general achieved.

In the setting of Quermass model, it is in general not possible to compute $C_\Lambda^{z,\theta}(\omega; f)$ given the observation $\mathcal{U}_\omega \cap \Lambda$. Consider for instance the pseudo-likelihood estimator. It is a particular case of the Takacs Fiksel procedure where $f_k = \partial h^\theta((x, R), \omega) / \partial \theta_k$, $k = 1, 2, 3$

and $f_4 = 1/z$ (see section 3.2 in [3]). In this case the computation of (3.1) requires the observation of all marked points in ω_Λ and so the pseudo-likelihood procedure is not feasible. However, it is possible to find some test functions f such that

1. for all $x \in \Lambda$ and $R \in [0, R_0]$, $f((x, R), \omega)$ is computable, making the integral term in (3.1) calculable,
2. the sum term in (3.1) is computable from the observation of $\mathcal{U}_\omega \cap \Lambda$ only.

Some examples are provided below.

Note finally that for any $x \in \Lambda$ and any $R \in [0, R_0]$ the computation of the local energy $h^\theta((x, R), \omega)$ is always possible (up to some possibly edge effects discussed in Section 4.3). Indeed, denoting $\tilde{\mathcal{U}}(x, R) = \mathcal{U}_\omega \cap B(x, R)$, the additivity of \mathcal{A} , \mathcal{L} and χ implies that

$$h^\theta((x, R), \omega) = \theta_1 \left[\pi R^2 - \mathcal{A}(\tilde{\mathcal{U}}(x, R)) \right] + \theta_2 \left[2\pi R - \mathcal{L}(\tilde{\mathcal{U}}(x, R)) \right] + \theta_3 \left[1 - \chi(\tilde{\mathcal{U}}(x, R)) \right]. \quad (3.3)$$

3.2.2 Some well-adapted test functions

In this section, we introduce some test functions f that make $C_\Lambda^{z, \theta}(\omega; f)$ in (3.1) computable from the observation of $\mathcal{U}_\omega \cap \Lambda$ only. This provides a solution for estimation in the Quermass model in spite of its unobservability issue. We restrict our presentation here to the case $\omega = \omega_\Lambda$, or equivalently $\Lambda' = \Lambda$, meaning that the observation window coincides with the domain of definition of P^{z^*, θ^*} . The general case involves some edge effects which are discussed in Section 4.3.

Let us first consider the test function f_0 defined by

$$f_0((x, R), \omega) = \text{Length} \left(\mathcal{S}(x, R) \cap (\mathcal{U}_\omega)^c \right), \quad (3.4)$$

where $\mathcal{S}(x, R)$ is the sphere with centre x and radius R . The quantity $f_0((x, R), \omega)$ is actually the length of arcs from the sphere $\mathcal{S}(x, R)$ which are outside \mathcal{U}_ω . Although the quantity $f_0((x, R), \omega \setminus (x, R))$ is not observable for any (x, R) in ω_Λ , the sum over $(x, R) \in \omega_\Lambda$ is nothing else than the total perimeter of $\mathcal{U}_{\omega_\Lambda}$:

$$\sum_{x \in \omega_\Lambda} f_0((x, R), \omega \setminus (x, R)) = \mathcal{L}(\mathcal{U}_{\omega_\Lambda}). \quad (3.5)$$

Moreover, it is possible to compute $f_0((x, R), \omega)$ for any $x \in \Lambda$ and $R \in [0, R_0]$, making the integral in (3.1) calculable. It follows that $C_\Lambda^{z, \theta}(\omega; f_0)$ is computable.

Similarly for any $\alpha > 0$, we consider the test function

$$f_\alpha((x, R), \omega) = \text{Length} \left(\mathcal{S}(x, R + \alpha) \cap (\mathcal{U}_\omega \oplus B(0, \alpha))^c \right), \quad (3.6)$$

where $\mathcal{U}_\omega \oplus B(0, \alpha)$ denotes the α -parallel set of \mathcal{U}_ω defined by the Minkowski sum of \mathcal{U}_ω and $B(0, \alpha)$. In this case (3.1) is also computable and the sum therein reduces to the perimeter of the α -parallel set:

$$\sum_{x \in \omega_\Lambda} f_\alpha((x, R), \omega \setminus (x, r)) = \mathcal{L}(\mathcal{U}_{\omega_\Lambda} \oplus B(0, \alpha)). \quad (3.7)$$

In the same spirit as (3.5), it is natural to look for some test functions f_{area} and f_{ep} such that the sum in (3.1) respectively reduces to $\mathcal{A}(\mathcal{U}_{\omega_\Lambda})$ and $\chi(\mathcal{U}_{\omega_\Lambda})$, and on the other hand the integral term in (3.1) is calculable. Unfortunately, we have not found any. Nevertheless, considering the test function

$$f_{\text{sum}} = \sum_i f_{\alpha_i}, \quad (3.8)$$

where the sum is done over some suitable finite set of non negative α_i 's, we obtain

$$\sum_{x \in \omega_\Lambda} f_{\text{sum}}((x, R), \omega \setminus (x, r)) = \sum_i \mathcal{L}(\mathcal{U}_{\omega_\Lambda} \oplus B(0, \alpha_i)), \quad (3.9)$$

which is closely related to the area of the complementary of $\mathcal{U}_{\omega_\Lambda}$ in Λ , see Figure 2. For this reason, f_{sum} can be viewed as a substitute for f_{area} .

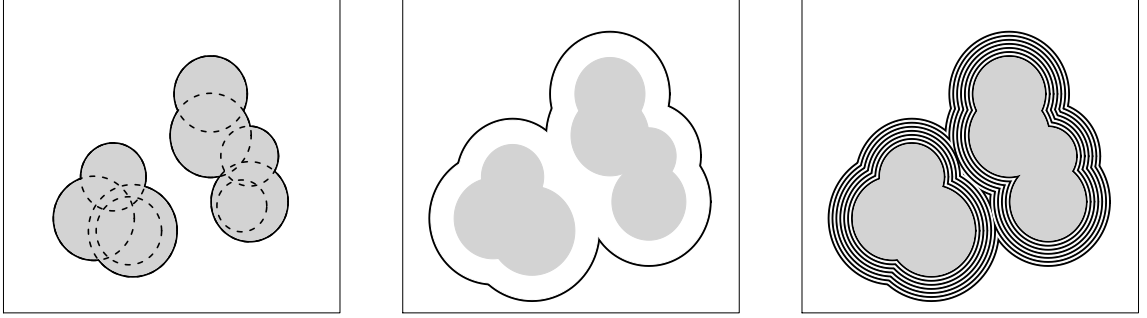


Figure 2: Left: $\mathcal{U}_{\omega_\Lambda}$ in gray, as the union of the balls bordered with dashed lines; the length of the solid black line is the quantity (3.5). Middle: same $\mathcal{U}_{\omega_\Lambda}$ in gray; the length of the solid black line is the quantity (3.7) for some $\alpha > 0$. Right: same $\mathcal{U}_{\omega_\Lambda}$ in gray; the sum of lengths of the solid black lines is the quantity (3.9) for 7 α_i 's.

Let us finally introduce the test function f_{iso} which indicates, for any $(x, R) \in \omega_\Lambda$, whether $B(x, R)$ is an isolated ball in \mathcal{U}_ω :

$$f_{\text{iso}}((x, R), \omega) = \begin{cases} 1 & \text{if } \mathcal{S}(x, R) \cap \mathcal{U}_\omega = \emptyset, \\ 0 & \text{otherwise.} \end{cases} \quad (3.10)$$

In this case, $\sum_{x \in \omega_\Lambda} f_{\text{iso}}((x, R), \omega \setminus (x, R))$ is the number of isolated balls in $\mathcal{U}_{\omega_\Lambda}$. Let us note that an isolated ball can contain smaller balls completely included inside it.

Remark 3.1. *The test functions $f_0, f_\alpha, f_{\text{sum}}, f_{\text{iso}}$ introduced above satisfy all the regularity conditions assumed in [3], which implies consistency and asymptotic normality of associated TF estimators, provided identifiability holds (see Section 4.4).*

4 Practical aspects of TF estimation

4.1 Computation of the contrast function

The TF estimator in (3.2) requires to compute $C_\Lambda^{z, \theta}(\omega; f)$ in (3.1) for the different well-adapted test functions f introduced in Section 3.2.2. Note that Section 4.3 explains how

handling edge effects in the computation of (3.1), so we don't address this question in this section.

The integral term in (3.1) can be approximated by a Monte Carlo approach, based on N independent points x_1, \dots, x_N uniformly distributed on Λ and N independent realisations R_1, \dots, R_N from μ . This leads to the approximation

$$C_\Lambda^{z,\theta}(\omega; f) \approx \sum_{x \in \omega_\Lambda} f((x, R), \omega \setminus (x, R)) - \frac{1}{N} \sum_{i=1}^N z e^{-h^\theta((x_i, R_i), \omega)} f((x_i, R_i), \omega). \quad (4.1)$$

Let us focus on the computation of (4.1) for the test functions f_0 , f_α , f_{sum} and some fixed values of z and θ . The first sum above reduces respectively to the perimeter of $\mathcal{U}_{\omega_\Lambda}$, the perimeter of the α -parallel set of $\mathcal{U}_{\omega_\Lambda}$, or the sum of such perimeters. The construction of α -parallel sets of $\mathcal{U}_{\omega_\Lambda}$ and the calculation of the above-mentioned perimeters may be achieved using some mathematical morphology tools, see e.g. [22], [20], [26]. The second sum in (4.1) involves the local energy of each new ball (x_i, R_i) , given by (3.3), and $f((x_i, R_i), \omega)$, for $f = f_0, f_\alpha, f_{\text{sum}}$. While for each i we can use again some mathematical morphology tools to calculate these two terms, the computation for the whole sum, which requires to repeat N times these calculations, may become difficult to implement.

An alternative procedure to compute (4.1) is to approximate the observed set $\mathcal{U}_\omega \cap \Lambda$ by any union of balls (e.g. by the procedure described in [29]) and to consider the associated power tessellation (see [17]). Then the construction of approximated α -parallel sets of $\mathcal{U}_{\omega_\Lambda}$ becomes straightforward since it suffices to increase the radius of each ball by α . Moreover, the calculation of the above-mentioned perimeters, the calculation of the local energy of any new ball (x_i, R_i) , and the calculation of $f((x_i, R_i), \omega)$, for $f = f_0, f_\alpha, f_{\text{sum}}$, are easily deduced from the associated power tessellations as described in [17].

We emphasize that the above procedure does not depend on the union of balls used to approximate $\mathcal{U}_\omega \cap \Lambda$. In order to minimize the computational complexity, an approximation involving a low number of balls is therefore preferable. Moreover, this union of balls is only used for computational reasons and has nothing to play with the germ-grain representation of \mathcal{U}_ω that we aim at fitting. In particular, the number of balls in this approximation is not relevant to estimate z^* .

Finally, let us focus on the computation of (4.1) for the test function f_{iso} . Contrary to f_0 , f_α and f_{sum} , the test function f_{iso} is strongly related to the ball structure of the germ-grain model, since the first sum in (4.1) corresponds to the number of isolated balls in $\mathcal{U}_{\omega_\Lambda}$. In this sense f_{iso} seems less natural for applications. However, as it will be demonstrated in Section 5, the test function f_{iso} appears to provide a relevant information for the estimation issue. For this reason, it can be important to include it in (3.2). In practice, we have then to decide what is considered as an isolated ball. A solution can be to consider an isolated component of $\mathcal{U}_{\omega_\Lambda}$ as an isolated ball, if its diameter is smaller than some constant chosen a priori. Another solution is to use the approximation of $\mathcal{U}_\omega \cap \Lambda$ by a union of balls, as mentioned above: an isolated component can then be considered as an isolated ball if it is approximated by an isolated ball.

In this work, the practical implementation of the TF procedure has been conducted using an approximation of $\mathcal{U}_\omega \cap \Lambda$ by a union of balls and the construction of the associated power tessellation.

4.2 Minimisation of the contrast function

As described in section 3.2.2, many computable test functions are available to implement the TF procedure for the Quermass model: f_0 , f_α for any $\alpha > 0$, f_{sum} , f_{iso} .

In order to estimate p unknown parameters among z^* , θ_1^* , θ_2^* and θ_3^* , the law of the radii μ being fixed, it suffices to choose $K \geq p$ test functions as above and to solve (3.2) where $\theta = (\theta_1, \theta_2, \theta_3)$.

The TF optimization (3.2) in z can be done explicitly. We deduce that the solution $(\hat{z}, \hat{\theta})$ of (3.2) necessarily belongs to the implicit manifold $z = \tilde{z}(\theta)$ where

$$\tilde{z}(\theta) := \frac{\sum_{k=1}^K S_k I_k(\theta)}{\sum_{k=1}^K I_k(\theta)}, \quad (4.2)$$

$$S_k = \sum_{x \in \omega_\Lambda} f_k((x, R), \omega \setminus (x, R))$$

and

$$I_k(\theta) = \int_0^{R_0} \int_\Lambda e^{-h^\theta((x, R), \omega)} f_k((x, R), \omega) dx \mu(dR).$$

Therefore, in practice, θ is first estimated by the solution $\hat{\theta}$ of (3.2) where z is replaced by $\tilde{z}(\theta)$, i.e.

$$\hat{\theta} = \arg \min_{\theta} \sum_{k=1}^K (S_k - \tilde{z}(\theta) I_k(\theta))^2.$$

This solution may be obtained by a grid search optimization procedure. Then z is estimated by $\hat{z} = \tilde{z}(\hat{\theta})$.

Note that the practical computation of all terms involved in (4.2) and (3.2) can be conducted as explained in Section 4.1.

This procedure allows to consider several estimators, depending on the number and the choice of test functions used in (3.2). It is not easy to find an optimal choice. The asymptotic variance of TF estimators is known (cf [3]), but appears intractable to be optimized. Some simulations are thus mandatory to provide some recommendations, see Section 5.

4.3 Edge effects

Based on the observation of $\mathcal{U}_\omega \cap \Lambda$, two types of edge effects may occur in the computation of (3.1) or (4.1).

First, edge effects may occur in the integral term in (3.1), or the second sum in (4.1), for the computation of $h^\theta((x, R), \omega)$ and $f((x, R), \omega)$, for $f = f_0, f_\alpha, f_{\text{sum}}$, or f_{iso} , when x is close to the boundary of Λ . In view of (3.3), (3.4), (3.6), (3.8), (3.10), this type of edge effects does not occur for the marked points (x, R) such that $B(x, R_{\text{max}}) \subset \Lambda$, where $R_{\text{max}} = R_0 + \max_i \alpha_i$. Therefore, in practice, this first type of edge effects can be avoided by considering the estimation on Λ^- , where Λ^- denotes the eroded set of Λ by R_{max} . The estimators are then defined by (3.2) where Λ is replaced by Λ^- .

Second, edge effects can occur for the first sum term in (3.1) and (4.1). Let us consider $f = f_0$. If $\omega = \omega_\Lambda$, as it was assumed for simplicity in Section 3.2.2, then from (3.5)

this sum term reduces to $\mathcal{L}(\mathcal{U}_{\omega_\Lambda})$. As we only observe $\mathcal{U}_\omega \cap \Lambda$, an approximation in this case could be $\mathcal{L}(\mathcal{U}_\omega \cap \Lambda)$ and we have $\mathcal{L}(\mathcal{U}_\omega \cap \Lambda) \leq \mathcal{L}(\mathcal{U}_{\omega_\Lambda})$, where the equality occurs if and only if $\mathcal{U}_\omega \subset \Lambda$. In the general case when $\omega \neq \omega_\Lambda$, the equality (3.5) does not hold any more and some extra terms due to edge effects have to be added in the right hand side of (3.5). Furthermore, to avoid the first type of edge effects, the estimation procedure is implemented on the eroded domain Λ^- . In this general case we may also use the approximation

$$\sum_{x \in \omega_{\Lambda^-}} f_0((x, R), \omega \setminus (x, R)) \approx \mathcal{L}(\mathcal{U}_\omega \cap \Lambda^-), \quad (4.3)$$

where the last perimeter can be computing by some mathematical morphology tools. Alternatively, $\mathcal{U}_\omega \cap \Lambda$ can be approximated by a union of balls, as suggested in Section 4.1, namely for some integer n , $\mathcal{U}_\omega \cap \Lambda \approx \bigcup_{i=1}^n B(y_i, r_i)$ where $y_i \in \Lambda$ and $r_i > 0$, and we can use the approximation

$$\sum_{x \in \omega_{\Lambda^-}} f_0((x, R), \omega \setminus (x, R)) \approx \sum_{y_i \in \Lambda^-} \text{Length} \left(\mathcal{S}(y_i, r_i) \cap \left(\bigcup_{\substack{j=1 \\ j \neq i}}^n B(y_j, r_j) \right)^c \right). \quad (4.4)$$

This last sum can easily be implemented from the power tessellation based on $\bigcup_{i=1}^n B(y_i, r_i)$.

Note that error of approximations in (4.3) and (4.4) involve only edge effects that become negligible when Λ tends to \mathbb{R}^2 . Finally similar approximations can be used for $f = f_\alpha, f_{\text{sum}}$ or f_{iso} instead of $f = f_0$ and we omit the details.

In this work, we have decided to handle edge effects by working in (3.2) with the eroded domain Λ^- instead of Λ , and by using the approximation (4.4), which is in agreement with our choice made to compute easily in practice the contrast terms (4.1).

4.4 Identifiability

The consistency of the TF procedure crucially depends on an identifiability assumption which basically implies that the contrast function in (3.2) has a unique minimum when Λ tends to \mathbb{R}^2 (see [3]). This assumption is in general satisfied if $K > p$, where p is the number of parameters to estimate. When $K = p$, identifiability is not easy to check, but has been proved to hold in some cases (see Example 2 in [3]).

Nevertheless, these theoretical considerations only ensure *asymptotic* identifiability. In practice, where $\Lambda \neq \mathbb{R}^2$, several local minima of the contrast function in (3.2) may arise and the global minimum might lead to an improper estimation. To avoid such drawback, a solution is to consider several TF contrast functions, coming from various choice of test functions. They should all share a local minimum in the same region, which allows us to restrict the domain of optimization.

5 Simulations

5.1 Estimation of the intensity parameter z^*

Let us first assume that $\theta_1^*, \theta_2^*, \theta_3^*$ are known and let us focus on the estimation of z^* , which appears as the main challenge for the Quermass model. In this setting, the equation (4.2) with $\theta = \theta^*$ provides an explicit estimator of z^* . The computation of (4.2) is conducted

as explained in Section 4: we focus on an eroded domain to prevent edge effects and the Monte Carlo approximation (4.1) is applied, where we choose $N = 2500$.

More specifically, we consider the estimators $\hat{z}_0, \hat{z}_{\alpha_1}, \dots, \hat{z}_{\alpha_{10}}, \hat{z}_{\text{iso}}$ and \hat{z}_{sum} , defined by (4.2) where $K = 1$ and where f_k is respectively $f_0, f_{\alpha_1}, \dots, f_{\alpha_{10}}, f_{\text{iso}}$ and f_{sum} . The latest test function f_{sum} is defined by the sum (3.8) over the ten previous $\alpha_i, i = 1, \dots, 10$.

Some results for the estimation of z^* are displayed in Figure 3, based on 100 replicates of the Area process ($\theta_2^* = 0, \theta_3^* = 0$) on $[0, 50]^2$, when $z^* = 0.1, \theta_1^* = 0.2$ and μ is the uniform law on $[.5, 2]$. The left plot is concerned with large parallel sets: $\alpha_i = i/5, i = 1, \dots, 10$, while the right plot involves small parallel sets: $\alpha_i = i/50, i = 1, \dots, 10$.

Figure 3 confirms that our procedure allows to estimate z in presence of the unobservability issue. Moreover, it appears that small parallel sets seem to provide better estimates. The same conclusion holds from intensive estimations of z^* for other values of θ_1^*, θ_2^* and θ_3^* (omitted in this article).

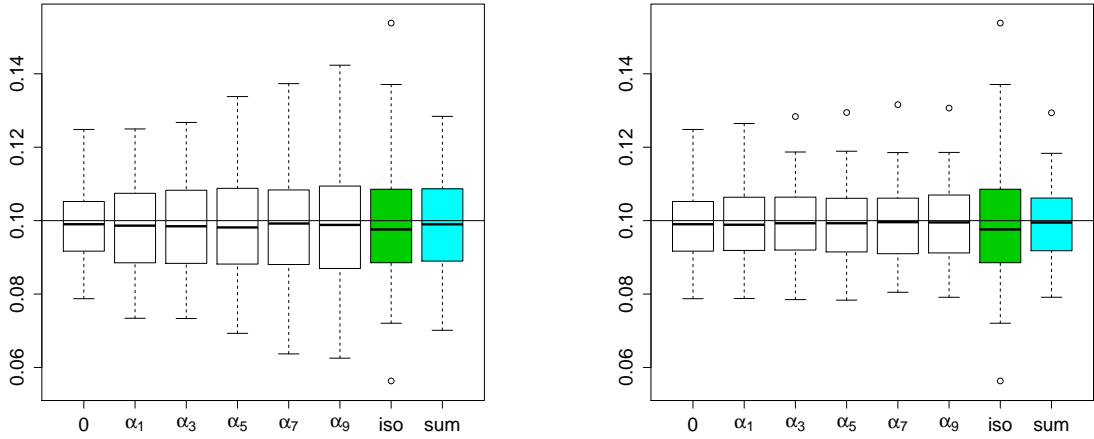


Figure 3: Estimations of $z^* = 0.1$ from 100 replicates of an Area process ($\theta_1^* = 0.2$). Left: boxplots of $\hat{z}_0, \hat{z}_{\alpha_i}$ ($\alpha_i = i/5$), \hat{z}_{iso} and \hat{z}_{sum} . Right: same boxplots but with $\alpha_i = i/50$.

5.2 Estimation for the \mathcal{A}, \mathcal{L} and χ process

In this section, we consider estimation in the Area process ($\theta_2^* = \theta_3^* = 0$), in the Perimeter process ($\theta_1^* = \theta_3^* = 0$) and in the Euler-Poincaré process ($\theta_1^* = \theta_2^* = 0$). In these cases, two parameters have to be estimated: the interacting parameter (θ_1^*, θ_2^* or θ_3^*) and the intensity parameter z^* .

Many TF estimators are conceivable. For instance, for the Area process, the estimation of (z^*, θ_1^*) can be achieved by the following TF estimators with $K = 2$: $(\hat{z}_{\text{iso}}, \hat{\theta}_{\text{iso}})$ based on (f_0, f_{iso}) ; $(\hat{z}_{\alpha}, \hat{\theta}_{\alpha})$ based on (f_0, f_{α}) for some $\alpha > 0$; $(\hat{z}_{\text{sum}}, \hat{\theta}_{\text{sum}})$ based on (f_0, f_{sum}) where the sum (3.8) is done over ten α_i 's. It is also possible to consider more test functions, as for example with $K = 11$: $(\hat{z}_{\text{all}}, \hat{\theta}_{\text{all}})$ based on $f_0, f_{\alpha_1}, \dots, f_{\alpha_{10}}$ for ten different α_i 's.

Some simulations (omitted here) show that the estimations $(\hat{z}_{\alpha}, \hat{\theta}_{\alpha})$ may be very variable depending on α for a given observation $\mathcal{U}_{\omega_{\Lambda}}$, even when using small parallel sets as

suggested in section 5.1. As far as we do not know which estimator is the most efficient, we prefer to use estimators that combine several small parallel sets. For this reason, we will concentrate on $(\hat{z}_{\text{sum}}, \hat{\theta}_{\text{sum}})$ and $(\hat{z}_{\text{all}}, \hat{\theta}_{\text{all}})$.

Another natural way to combine information coming from various parallel sets is to consider an aggregated estimator. How to aggregate several estimators is an interesting but difficult question, particularly in presence of strong dependent observations as in the Quermass model. We simply consider here the median of several estimators, that provides a natural robust combination:

$$(\hat{z}_{\text{med}}, \hat{\theta}_{\text{med}}) = \text{median}((\hat{z}_{\alpha_1}, \hat{\theta}_{\alpha_1}), \dots, (\hat{z}_{\alpha_{10}}, \hat{\theta}_{\alpha_{10}})).$$

Therefore, the following simulations focus on the three estimators: $(\hat{z}_{\text{sum}}, \hat{\theta}_{\text{sum}})$, $(\hat{z}_{\text{med}}, \hat{\theta}_{\text{med}})$ and $(\hat{z}_{\text{all}}, \hat{\theta}_{\text{all}})$, where $\alpha_i = i/50$, $i = 1, \dots, 10$. Moreover, since the test function f_{iso} plays a particular role as it is strongly related to the ball structure of the germ-grain model, we also assess the performance of $(\hat{z}_{\text{iso}}, \hat{\theta}_{\text{iso}})$, based on (f_0, f_{iso}) .

All simulations are done on $[0, 50]^2$. The law of radii μ is uniform on $[.5, 2]$. The practical implementation is conducted as explained in Section 4, that includes erosion and the Monte Carlo approximation (4.1). Figure 4 displays the estimation results on 100 replicates of, respectively: the Area process with $z^* = 0.1$, $\theta_1^* = 0.2$; the Perimeter process with $z^* = 0.2$, $\theta_2^* = 0.4$; and the Euler-Poincaré process with $z^* = 0.1$, $\theta_3^* = 1$.

As a first conclusion, we see from these simulations that all estimators considered in these simulations allow to estimate the two parameters and perform more or less equivalently. However, $(\hat{z}_{\text{all}}, \hat{\theta}_{\text{all}})$ seems to slightly surpass the other estimators, in terms of dispersion and outliers.

5.3 Estimation for the full Quermass process

To deal with the estimation of more interacting parameters, we proceed according to the previous conclusion. Given ten small α_i 's, we consider the TF estimator based on all available test functions $f_0, f_{\alpha_1}, \dots, f_{\alpha_{10}}, f_{\text{sum}}$ and f_{iso} . Since f_{iso} may be artificial to compute in practice (see Section 4.1), we also consider the TF estimator based on all previous test functions except f_{iso} .

Some results of estimation are presented in Figure 6 for 100 replicates of the $(\mathcal{A}, \mathcal{L})$ -process ($\theta_3^* = 0$) on $[0, 50]^2$, with $z^* = 0.1$, $\theta_1^* = -0.2$, $\theta_2^* = 0.3$ and the law of radii is uniform on $[.5, 2]$. The same kind of results are displayed in Figure 7 for the full Quermass process with $z^* = 0.1$, $\theta_1^* = -0.2$, $\theta_2^* = 0.3$ and $\theta_3^* = -1$. See some examples of samples in Figure 5.

While the quality of estimation turns to be satisfactory in presence of one interacting parameter (i.e. for the \mathcal{A} -process, the \mathcal{L} -process or the \mathcal{E} -process) as seen in Section 5.2, it naturally decreases in presence of more interacting parameters (Figure 6), to become very variable for the full Quermass model (Figure 7). Moreover, Figure 6 shows that the presence of the test function f_{iso} seems to improve the estimation, even if its computation in practice might appear artificial.

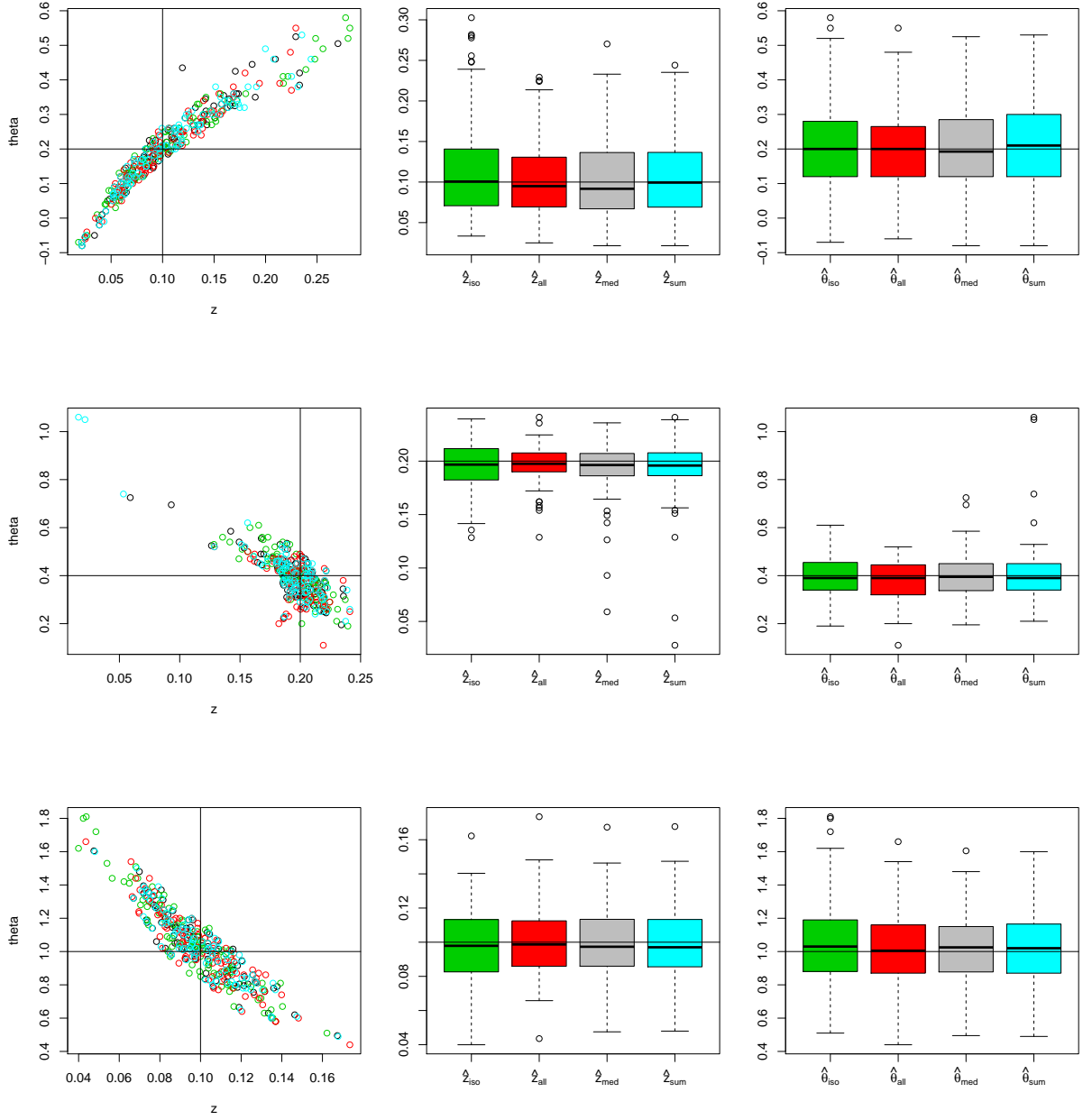


Figure 4: Estimations from 100 replicates of, from top to bottom: the \mathcal{A} -process ($z^* = 0.1$, $\theta_1^* = 0.2$); the \mathcal{L} -process ($z^* = 0.2$, $\theta_2^* = 0.4$); the χ -process ($z^* = 0.1$, $\theta_3^* = 1$). The estimators are $(\hat{z}_{\text{iso}}, \hat{\theta}_{\text{iso}})$ (green), $(\hat{z}_{\text{all}}, \hat{\theta}_{\text{all}})$ (red), $(\hat{z}_{\text{med}}, \hat{\theta}_{\text{med}})$ (black) and $(\hat{z}_{\text{sum}}, \hat{\theta}_{\text{sum}})$ (blue). From left to right: scatterplot of $(\hat{z}, \hat{\theta})$; boxplots of \hat{z} ; boxplots of $\hat{\theta}$.

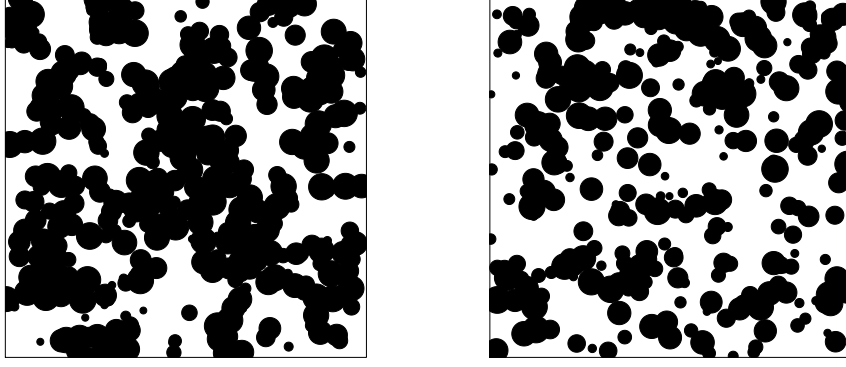


Figure 5: Samples of the $(\mathcal{A}, \mathcal{L})$ -process with $z^* = 0.1$, $\theta_1^* = -0.2$ and $\theta_2^* = 0.3$ (left) and of the Quermass process with $z^* = 0.1$, $\theta_1^* = -0.2$, $\theta_2^* = 0.3$ and $\theta_3^* = -1$ (right). The window is $[0, 50]^2$ and the radii are uniformly distributed on $[\frac{1}{2}, 2]^2$.

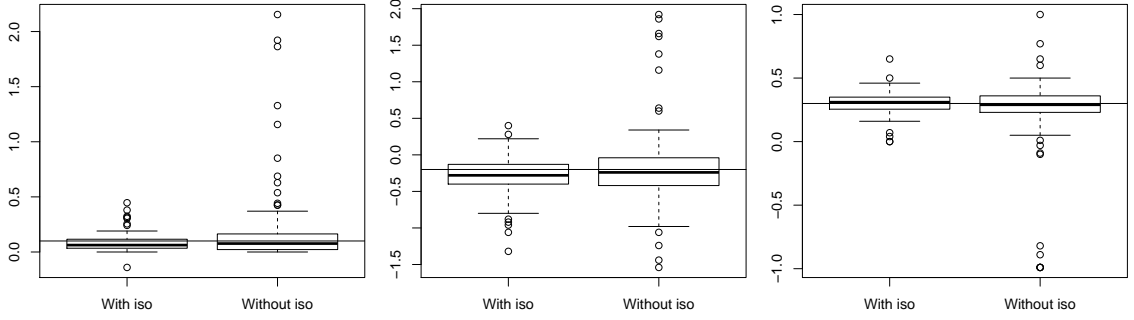


Figure 6: Estimation of z^* (left), θ_1^* (middle) and θ_2^* (right) from 100 replicates of the $(\mathcal{A}, \mathcal{L})$ -process with $z^* = 0.1$, $\theta_1^* = -0.2$ and $\theta_2^* = 0.3$. In each plot, the estimator involves f_{iso} (on the left) or not (on the right).

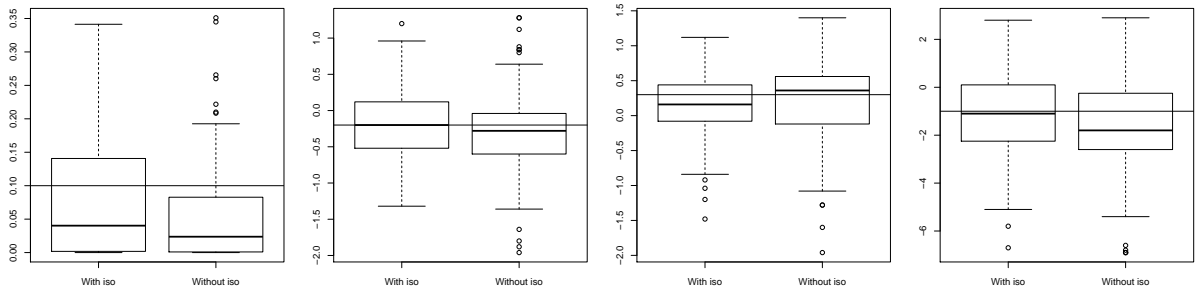


Figure 7: Estimation (from left to right) of z^* , θ_1^* , θ_2^* and θ_3^* from 100 replicates of the Quermass process with $z^* = 0.1$, $\theta_1^* = -0.2$, $\theta_2^* = 0.3$ and $\theta_3^* = -1$. In each plot, the estimator involves f_{iso} (on the left) or not (on the right).

6 Application to heather data

The plot on the left hand of Figure 8 shows a binary image of the presence of heather in a 10×20 m rectangular region at Jädraås, Sweden. This heather dataset has been widely studied. It was first presented by P. Diggle in [6], where it has been modelled by a stationary spherical Boolean model. This point of view has been considered further in [11, 12] and in [4], where alternative estimation methods for the Boolean model have been implemented.

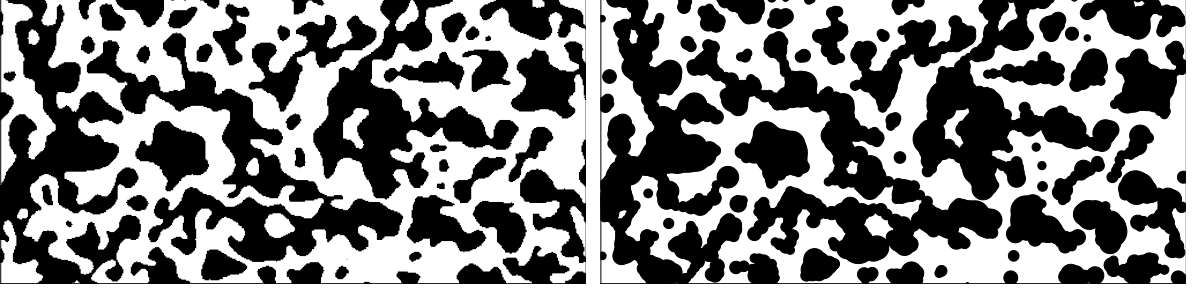


Figure 8: Heather data (left) and its approximation by a union of balls (right)

Considering heather bushes as discs, the spherical germ-grain representation of the data seems to be a natural approximation. However, the independance between the location of the grains and their radii, implied by the Boolean model, appears more questionable. As a matter of fact, simulations of the fitted Boolean models from the aforementioned studies do not look visually similar to the heather dataset, as initially observed by P. Diggle in [6]. This lack of fit has been confirmed in [18] by various diagnostic plots (as in Figure 9). The same conclusion is made in [19], where a Matérn's cluster model is proposed as an alternative to the Boolean model. However no estimation procedure for this Matérn's cluster model is given in [19]. Instead, a brute-force approach is used to choose the parameters in order to pass some diagnostic plots. While the latter model appears well adapted to the heather dataset, a comparison between our statistical method and the approach in [19] is therefore difficult and will not be conducted further.

Alternatively, a model of interacting discs has been fitted to the heather dataset in [18]. The model is very similar to the Quermass model, except that in the Hamiltonian (2.1), the Euler characteristic is replaced by the number of connected components. This model has been fitted in [18] by a maximum likelihood approach as described in Section 3.1, where three reference measures μ have been tested. As a result, the best fitted model was: μ is the uniform law on $[0, 0.53]$, $\hat{z} = 2.45$ and the estimated Hamiltonian, denoted $\tilde{H}^{\hat{\theta}}$, is

$$\tilde{H}^{\hat{\theta}}(\omega_{\Lambda}) = 4.91 \mathcal{A}(\mathcal{U}_{\omega_{\Lambda}}) - 1.18 \mathcal{L}(\mathcal{U}_{\omega_{\Lambda}}) + 2.25 \mathcal{N}_{cc}(\mathcal{U}_{\omega_{\Lambda}}), \quad (6.1)$$

where $\mathcal{N}_{cc}(\mathcal{U}_{\omega_{\Lambda}})$ denotes the number of connected components of $\mathcal{U}_{\omega_{\Lambda}}$.

As explained in Section 3.1, the estimation procedure used in [18] implies some rather strong restriction on the parameter space. For comparison, we fit hereafter a Quermass model to heather data using the TF approach.

Following the practical recommendations in Section 4, the binary image is first approximated by a union of balls, using the procedure described in [29]. The result of this approximation is shown on the right plot of Figure 8. Second, we choose for the reference

measure μ the uniform law on $[0.05, 0.55]$, which is in agreement with the final choice made in [18], except that a minimal value for the radii has been fixed to 0.05, corresponding to the smallest radius of the spots observed in heather dataset.

The estimation of the full Quermass model (i.e. all parameters $z, \theta_1, \theta_2, \theta_3$ are unknown) did not give satisfactory results. This is not very surprising in view of the strong variability of the estimates observed in Figure 7. The contrast function in (3.2) computed from the heather dataset actually exhibits in this general case a large amount of local minima, leading to an identifiability issue. After a deeper insight, it appears that any value of the intensity parameter z can somehow be compensated by some value of the area interaction parameter θ_1 . This identifiability issue between the area interaction and the intensity is well-known: it is already visible in the top-left plot of Figure 4, where we observe a strong correlation between the two estimates in the \mathcal{A} -process. Therefore, we have decided to focus on a simpler model. Since the heather dataset seems not rich enough to distinguish the role played by the intensity parameter z and the area interaction parameter θ_1 , a natural choice is to fit a (\mathcal{L}, χ) -process. As a matter of fact, fitting a $(\mathcal{A}, \mathcal{L})$ -process leads to the same kind of identifiability issue as before. This basically means that only one parameter becomes relevant in the $(\mathcal{A}, \mathcal{L})$ -process for the heather dataset, namely the perimeter interaction parameter, which is not sufficient to obtain a good fit.

So, the estimation of the (\mathcal{L}, χ) -process has been implemented on the balls approximations of heather dataset (right plot of Figure 8), using the TF procedure associated to the test functions $f_0, f_{\alpha_1}, \dots, f_{\alpha_{10}}, f_{\text{sum}}$ and f_{iso} , where $\alpha_i = 0.005 i, i = 1, \dots, 10$ and where μ is the uniform law on $[0.05, 0.55]$. As a result, we have obtained $\hat{z} = 2.12$ and

$$H^{\hat{\theta}}(\omega_{\Lambda}) = 0.14 \mathcal{L}(\mathcal{U}_{\omega_{\Lambda}}) + 0.22 \chi(\mathcal{U}_{\omega_{\Lambda}}). \quad (6.2)$$

In order to check the quality of fit of (6.2) to heather dataset, we propose some diagnostic plots in Figure 9, where a comparison is also provided with the fitted model (6.1) of [18]. These plots are the same as in [18], they correspond to an estimation of the contact distribution function (top left): $H(r) = P(D \leq r | D > 0)$ where $D = \inf\{\rho \geq 0 : \mathcal{U} \cap B(0, \rho) \neq \emptyset\}$; the covariance function (top right) $C(r) = P(x \in \mathcal{U}, y \in \mathcal{U}, \|x - y\| = r)$; and some shape-characteristics (see [24] or [18] for a definition): erosion e_r (middle left), dilatation d_r (middle right), opening o_r (bottom left) and closing c_r (bottom right). More specifically, all plots in Figure 9 show the simulated 95% envelopes obtained under (6.2) in solid black lines, the simulated 95% envelopes obtained under (6.1) in dashed black lines, the empirical estimates from heather dataset (in solid red lines) and from its balls approximation (red lines with circles).

A slight better fit is observed for (6.2), in particular from the contact distribution function, the erosion and the closing, even if the closing is not fitted very well. This conclusion seems confirmed by the visual impression from samples of (6.1) and (6.2), shown respectively in Figure 10 and 11, next to the balls approximation of heather dataset.

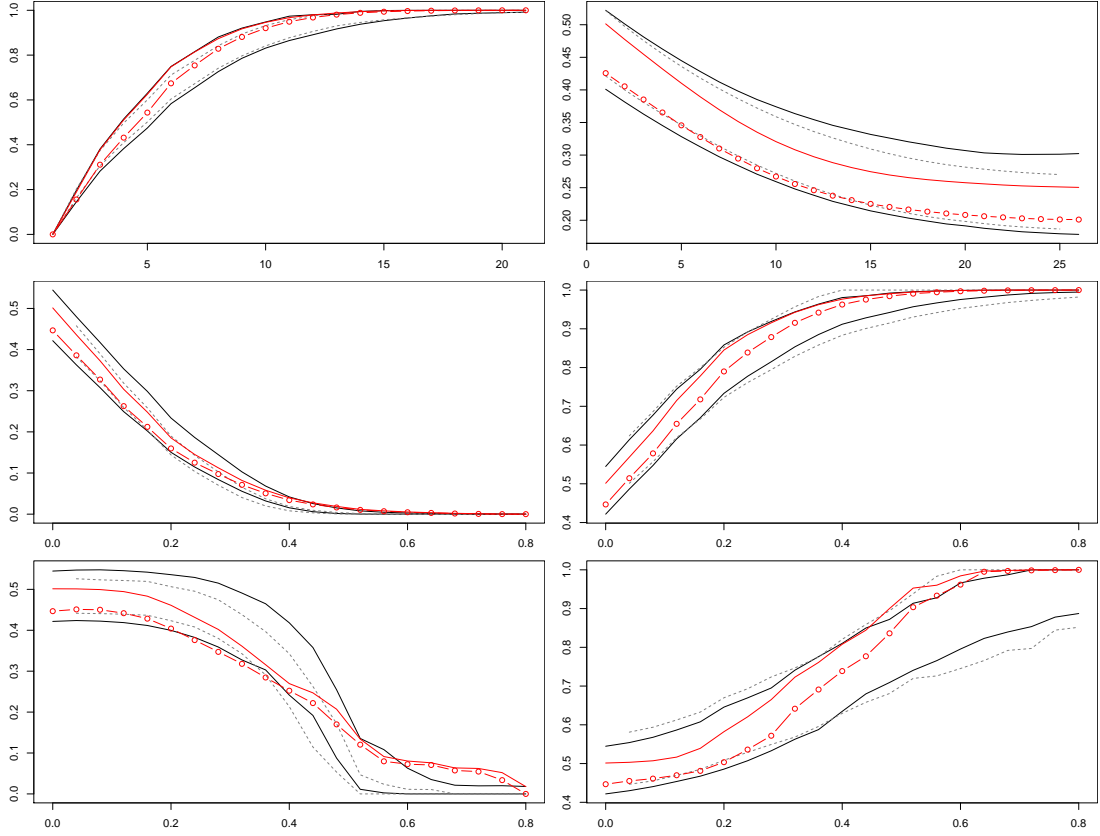


Figure 9: From top left to bottom right: contact distribution function, covariance function, erosion, dilatation, opening, closing, for the empirical estimation from heather dataset (solid red line), the empirical estimation for the balls approximation of heather dataset (red line with circles), 95% envelopes under (6.2) (solid black line), 95% envelopes under (6.1) (dashed black line)

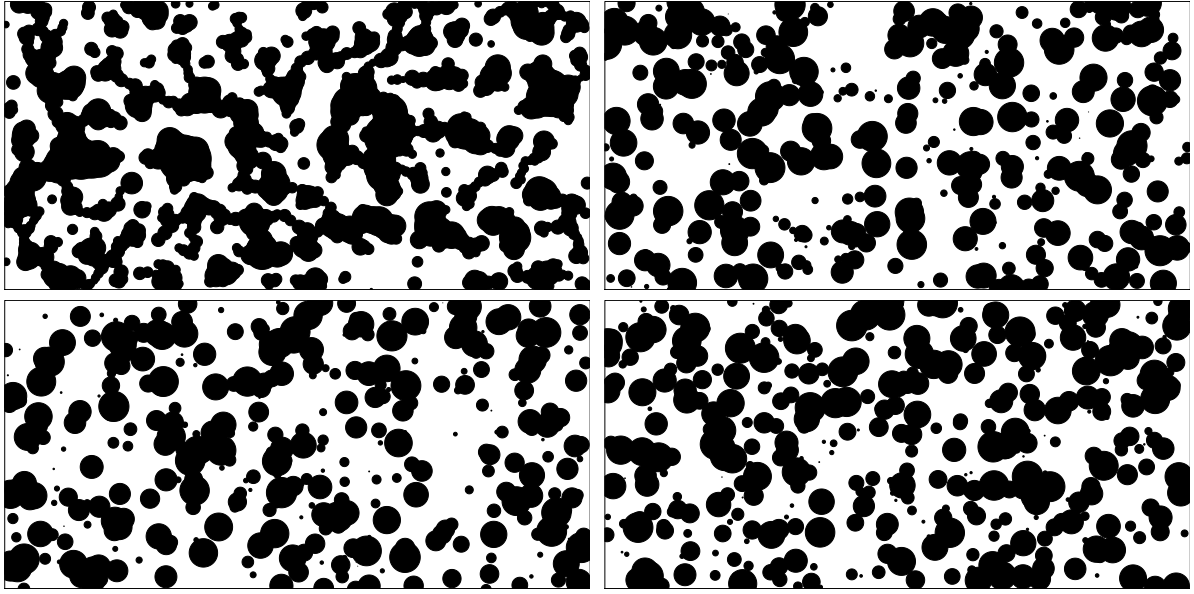


Figure 10: Heather data approximation (top left) and three samples from the fitted model (6.1)

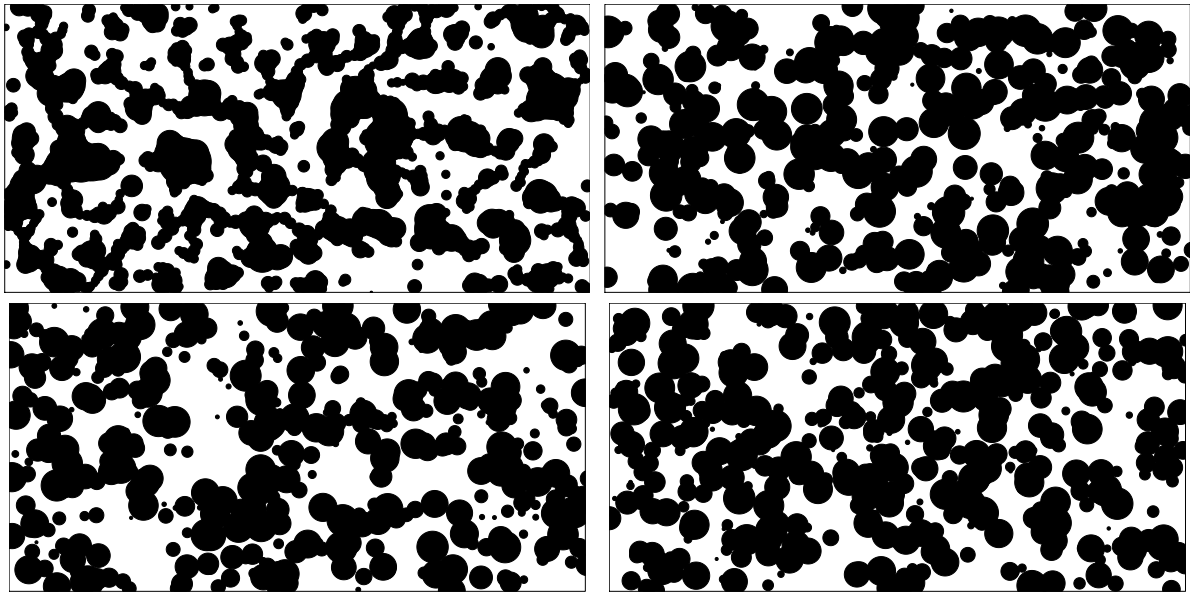


Figure 11: Heather data approximation (top left) and three samples from the fitted model (6.2)

Appendix: Combining MLE and TF approaches

The MLE is known to be an efficient method of estimation, but does not allow to estimate the parameter z^* in the Quermass model (see section 3.1). Moreover, the Takacs Fiksel procedure allows to estimate all parameters, given well-adapted test functions (see section 3.2). A natural idea is to try to combine these two approaches. Roughly speaking, we would like to first estimate z^* by the Takacs-Fiksel method, then estimate $\theta^* := (\theta_1^*, \theta_2^*, \theta_3^*)$ by MLE.

Let us first recall that, given K test functions, the solution $(\hat{z}, \hat{\theta})$ of the TF optimization procedure (3.2) necessarily belongs to the implicit manifold $z = \tilde{z}(\theta)$ given by (4.2) (see section 4).

On the other hand, the MLE $(\hat{z}, \hat{\theta})$ solves the estimating equations

$$\begin{cases} \mathbb{E}_{\hat{z}, \hat{\theta}}(n(\omega_\Lambda)) &= n(\omega_{\Lambda, \text{obs}}) \\ \mathbb{E}_{\hat{z}, \hat{\theta}}(\mathcal{A}(\mathcal{U}_{\omega_\Lambda})) &= \mathcal{A}(\mathcal{U}_{\omega_{\Lambda, \text{obs}}}) \\ \mathbb{E}_{\hat{z}, \hat{\theta}}(\mathcal{L}(\mathcal{U}_{\omega_\Lambda})) &= \mathcal{L}(\mathcal{U}_{\omega_{\Lambda, \text{obs}}}) \\ \mathbb{E}_{\hat{z}, \hat{\theta}}(\chi(\mathcal{U}_{\omega_\Lambda})) &= \chi(\mathcal{U}_{\omega_{\Lambda, \text{obs}}}) \end{cases} \quad (6.3)$$

where $\omega_{\Lambda, \text{obs}}$ and $\mathcal{U}_{\omega_{\Lambda, \text{obs}}}$ respectively denote the observed point configuration and the observed random set on Λ . Of course $n(\omega_{\Lambda, \text{obs}})$ is not available in practice and the system cannot be solved.

A way to combine the two procedures is to look for the best solution of (6.3) restricted to the implicit manifold $z = \tilde{z}(\theta)$. More specifically, θ^* is estimated by

$$\hat{\theta}_{\text{mix}} = \arg \min_{\theta} d \left(\mathbb{E}_{\tilde{z}(\theta), \theta}(\mathcal{A}(\mathcal{U}_{\omega_\Lambda}), \mathcal{L}(\mathcal{U}_{\omega_\Lambda}), \chi(\mathcal{U}_{\omega_\Lambda})), (\mathcal{A}(\mathcal{U}_{\omega_{\Lambda, \text{obs}}}), \mathcal{L}(\mathcal{U}_{\omega_{\Lambda, \text{obs}}}), \chi(\mathcal{U}_{\omega_{\Lambda, \text{obs}}})) \right), \quad (6.4)$$

where d is any distance function in \mathbb{R}^3 , and z is estimated by $\hat{z}_{\text{mix}} = \tilde{z}(\hat{\theta}_{\text{mix}})$.

In practice, it is necessary to approximate the expectations in (6.4), since their close expression is intractable. Let us focus on the expectation of $\mathcal{A}(\mathcal{U}_{\omega_\Lambda})$. A straightforward approach is to use Monte-Carlo approximations. Given N independent realisations $\omega_1, \dots, \omega_N$ of a Quermass process on Λ with parameters z and θ , we have, for N large enough,

$$\mathbb{E}_{z, \theta}(\mathcal{A}(\mathcal{U}_\omega)) \approx \frac{1}{N} \sum_{k=1}^N \mathcal{A}(\mathcal{U}_{\omega_k}). \quad (6.5)$$

This approximation requires to simulate a large number of Quermass realisations for each value of θ , which seems prohibitively time consuming in practice. An alternative approach is to use MCMC approximation. Let $\omega_1^0, \dots, \omega_N^0$ be N independent realisations of a Quermass process on Λ with fixed parameters z_0 and θ_0 . Then from the ergodic theorem, for any z and θ , it is not difficult to check that for N large enough

$$\mathbb{E}_{z, \theta}(\mathcal{A}(\mathcal{U}_\omega)) \approx \frac{\sum_{k=1}^N \mathcal{A}(\mathcal{U}_{\omega_k^0}) (z/z_0)^{n(\omega_k^0)} \exp[(\theta - \theta_0)\mathcal{A}(\mathcal{U}_{\omega_k^0})]}{\sum_{k=1}^N (z/z_0)^{n(\omega_k^0)} \exp[(\theta - \theta_0)\mathcal{A}(\mathcal{U}_{\omega_k^0})]}. \quad (6.6)$$

This approach should be quicker in practice than (6.5) because the simulation of N Quermass realisations has to be done only once and not for each value of θ . Unfortunately it

appears that the variance of the right hand side in (6.6) becomes very large when (z, θ) is not close to (z_0, θ_0) , making the convergence prohibitively slow. A solution is to change the initial value (z_0, θ_0) according to (z, θ) , but then the procedure loses its advantages in comparison with (6.5). Therefore, the approximations of the expectations in (6.4), whatever (6.5) or (6.6) is used, appears as a strong restriction to apply this mix procedure.

To assess the quality of the mix procedure anyway, we focus on the estimation of z^* and θ_1^* in the Area process. In (6.4), we simply choose the euclidean distance for d and the expectation is approximated by (6.5) so that

$$\hat{\theta}_{1,\text{mix}} = \arg \min_{\theta_1} \left| \frac{1}{N} \sum_{k=1}^N \mathcal{A}(\mathcal{U}_{\omega_k}(\tilde{z}(\theta_1), \theta_1)) - \mathcal{A}(\mathcal{U}_{\omega_{\Lambda}, \text{obs}}) \right|$$

where $\omega_k(\tilde{z}(\theta_1), \theta_1)$, $k = 1, \dots, N$ are independent realisations of an Area process with parameters $(\tilde{z}(\theta_1), \theta_1)$. The estimations have been implemented on the same realisations than in Section 5.2, see the first row of Figure 4, and with $N = 250$. The results are displayed in Figure 12.

As a conclusion, the mix procedure does not seem to perform better than the TF estimators considered in section 5.2. In view of the calculation time required for the approximations (6.5) or (6.6), we did not give preference to this procedure in this paper.

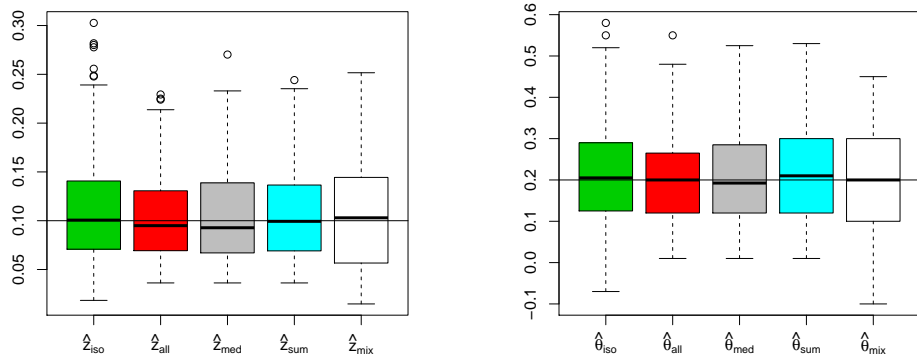


Figure 12: Estimations of z^* (left) and θ_1^* (right) for the Area process as in the first row of Figure 4 with, in addition, \hat{z}_{mix} and $\hat{\theta}_{1,\text{mix}}$ (in white).

References

- [1] A. BADDELEY and M. N. M. VAN LIESHOUT, *Area-interaction point processes*, Ann. Inst. Statist. Math, 47(4):601–619 (1995).
- [2] J.T. CHAYES, L. CHAYES and R. KOTECKY, *The Analysis of the Widom-Rowlinson Model by Stochastic Geometric methods*, Commun. math. Phys., 172:551–569 (1995).

- [3] J.-F. COEURJOLLY, D. DEREUDRE, R. DROUILHET and F. LAVANCIER, *Takacs Fiksel method for stationary marked Gibbs point processes*, to appear in Scand. J. of Stat.
- [4] N. CRESSIE, *Statistics for Spatial Data*. Wiley, New York, 2nd edition (1993).
- [5] D. DEREUDRE, *Existence of Quermass processes for non locally stable interaction and non bounded convex grains*, Adv. in Appl. Probab., 41:664–681 (2009).
- [6] P. DIGGLE, *Binary mosaics and the spatial pattern of heather*, Biometrics, 37:531–539 (1981).
- [7] T. FIKSEL, *Estimation of interaction potentials of Gibbsian point processes*, Statistics, 19:77–86 (1988).
- [8] H.-O. GEORGII, *Canonical and grand canonical Gibbs states for continuum systems*, Commun. Math. Phys., 48:31–51 (1976).
- [9] H.-O. GEORGII and T. KÜNETH, *Stochastic comparison of point random fields*, J. Appl. prob., 34:868–881 (1997).
- [10] H. HADWIGER, *Vorlesungen über Inhalt, Oberfläche und Isoperimetrie*, Springer, Berlin (1957).
- [11] P. HALL, *Counting methods for inference in binary mosaics*, Biometrics, 41:1049–1052 (1985).
- [12] P. HALL, *Introduction to the Theory of Coverage Processes*. Wiley, New York (1988).
- [13] W. S. KENDALL, M. N. M. VAN LIESHOUT and A. J. BADDELEY, *Quermass-interaction processes conditions for stability*, Adv. Appl. Prob., 31:315–342 (1999).
- [14] C. N. LIKOS, K. R. MECKE and H. WAGNER, *Statistical morphology of random interface microemulsions*, J. Chem. Phys., 93:9350–9361 (1995).
- [15] K. R. MECKE, *A morphological model for complex fluids*, J. Phys. Condens. Matter, 8:9663–9667 (1996).
- [16] I. MOLCHANOV, *Statistics of the Boolean Model for Practitioners and Mathematicians*, Wiley, Chichester (1997).
- [17] J. MØLLER and K. HELISOVA, *Power diagrams and interaction processes for unions of discs*, Advances in Applied Probability, 40:321–347 (2008).
- [18] J. MØLLER and K. HELISOVA, *Likelihood inference for unions of interacting discs*, Scandinavian Journal of Statistics, 37(3):365–381 (2010).
- [19] T. MRKVIČKA, *On testing of general random closed set model hypothesis*, Kybernetika, 45(2):293–308 (2009).

- [20] T. MRKVIČKA, J. RATAJ, *On estimation of intrinsic volume densities of stationary random closed sets*, Stoch. Proc. Appl., 118(2):213–231 (2008).
- [21] X.X. NGUYEN and H. ZESSIN, *Integral and differential characterizations of the Gibbs process*, Math. Nach., 88:105–115 (1979).
- [22] J. OHSER, F. MÜCKLICH, *Statistical Analysis of Microstructures in Materials Science*. Wiley, Chichester (2000).
- [23] C. PRESTON, *Random fields*, Lecture Notes in Mathematics 714, Springer, Berlin (1976).
- [24] B. D. RIPLEY, *Statistical Inference for Spatial Processes*. Cambridge University Press, Cambridge (1988).
- [25] D. RUELLE, *Statistical Mechanics, Rigorous Results*. Benjamin, New-York (1969).
- [26] V. SCHMIDT, E. SPODAREV, *Joint estimators for the specific intrinsic volumes of stationary random sets*, Stoch. Proc. Appl., 115:959–981 (2005).
- [27] D. STOYAN, W. S. KENDALL, J. MECKE, *Stochastic Geometry and its applications*, Wiley, New York (1995).
- [28] R. TAKACS, *Estimator for the pair-potential of a Gibbsian point process*, Math. Operationsforsch. u. Statist., ser. statist. 17: 428–433 (1986).
- [29] R. THIEDMANN, H. HASSFELD, O. STENZEL, L. KOSTER, S. OOSTERHOUT, S. VAN BAVEL, M. WIENK, J. LOOS, R. JANSSEN, V. SCHMIDT, *A multiscale approach to the representation of 3D images, with applications to polymer solar cells.*, Image Analysis & Stereology, 30(1): 19–30 (2011).
- [30] B. WIDOM and J. S. ROWLINSON, *New model for the study of liquid-vapor phase transitions*, J. Chem. phys., 52:1670–1684 (1970).